Heliyon 10 (2024) e37493

Contents lists available at ScienceDirect

Heliyon

journal homepage: www.cell.com/heliyon

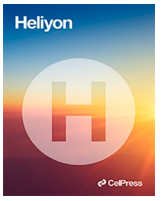

Research article

Optimization, molecular dynamics and quantum parameters simulations of *Zingiber officinale* rhizome as a green corrosion inhibitor

Olajire Samson Olanrele [a], Joseph Femi-Dagunro [a], Edwin Andrew Ofudje [a,*], Meri Algarni [b], Azza A. Al-Ghamdi [c], Reema H. Aldahiri [c], Mazen R. Alrahili [d], Ahad Amer Alsaiari [e]

[a] *Department of Chemical Sciences, Mountain Top University, Ogun State, Nigeria*
[b] *Department of Physics, Faculty of Science, Al-Baha University, Alaqiq, 65779-7738, Saudi Arabia*
[c] *Department of Chemistry, College of Science, University of Jeddah, Jeddah, 21959, Saudi Arabia*
[d] *Physics Department, School of Science, Taibah University, Medina, 42353, Saudi Arabia*
[e] *Department of Clinical Laboratory Science, College of Applied Medical Science, Taif University, Taif, Saudi Arabia*

ARTICLE INFO

Keywords:
Corrosion inhibition
Quantum chemical calculation
Zingiber officinale rhizome
Molecular dynamic
Mild steel

ABSTRACT

This study combines experimental and theoretical approaches to investigate ginger root extract (GRE) as an eco-friendly corrosion inhibitor for mild steel in acidic environments at temperatures ranging from 303 to 333 K. Experimental techniques, including weight loss measurements, were used to assess the inhibiting performance and adsorption behavior of GRE, while GC-MS, FT-IR, and UV–visible spectrophotometric methods provided further characterization. Results indicated that the inhibition efficiency of GRE increased with higher concentrations and decreased with temperature, highlighting its potential to effectively prevent corrosion in H_2SO_4 medium. GC-MS analysis identified four major phenolic compounds—6-gingerol, 6-isoshogaol, zingerone, and vanillyl glycol—and two secondary metabolites, α-Farnesene and β-Bisabolene. Among these, 6-gingerol, the most active and abundant constituent, was selected for computational studies. Optimal corrosion inhibition of 81.3 % was achieved at 303 K with a GRE concentration of 10 g/L for 1 h. Thermodynamic activation parameters suggested a temperature-dependent process, and alignment with the Langmuir isotherm indicated a physical adsorption mechanism. Quantum chemical calculations for 6-gingerol revealed highest occupied molecular orbital energy (E_{HOMO}) and lowest unoccupied molecular orbital energy (E_{LUMO}) values of -6.286 eV and -0.366 eV, respectively, in its protonated state, and -8.338 eV and -0.247 eV, respectively, in its neutral state. Molecular simulations showed a binding affinity of -4.736 kJ/mol between 6-gingerol and the steel surface, supporting the experimental findings and underscoring the potential of GRE as an effective corrosion inhibitor.

1. Introduction

Mild steel (MS) is widely employed in various industries, including manufacturing and petrochemicals, due to its exceptional

* Corresponding author.
E-mail address: ofudjeandrew4real@yahoo.com (E. Andrew Ofudje).

https://doi.org/10.1016/j.heliyon.2024.e37493
Received 3 July 2024; Received in revised form 3 September 2024; Accepted 4 September 2024
Available online 7 September 2024

mechanical properties and relatively low cost. However, MS is prone to corrosion due to its tendency to lose electrons easily during use, leading to the degradation of its metallographic structure. This corrosion reduces its functional value, causes economic losses, and introduces potential safety hazards [1–4]. In industrial production, to save costs, it is common to use strong acidic solutions for the pickling process to remove corrosion-induced oxides from MS [1–3]. While this method effectively eliminates surface oxides, it also induces a certain level of corrosion to the MS substrate [2–4]. Therefore, it is necessary to add corrosion inhibitors to the pickling solution to protect the MS substrate.

Corrosion inhibitors are broadly categorized into organic and inorganic types [5–9]. Inorganic inhibitors, such as chromates, have shown significant efficacy in the past. However, due to their carcinogenic and toxic properties, they have been banned in numerous countries [10]. Consequently, research has shifted towards organic inhibitors, also known as green corrosion inhibitors, which are efficient, cost-effective, and environmentally friendly [11–13]. These inhibitors work by binding to the metal substrate through phytochemicals containing polar functional groups, such as heteroatoms with lone pairs of electrons (e.g., N, S, O, and P), conjugated dienes, and aromatic structures, thereby reducing the corrosive impact of the acidic pickling solution on the MS substrate [7,11–14].

Ren et al. investigated pumpkin leaf extract (PLE) for mild steel corrosion prevention in 0.5M H_2SO_4. Electrochemical tests at different temperatures showed that the maximum concentration of extracts inhibited mild steel corrosion by more than 89.98 %. Quantum chemical calculations theoretically explained PLE's inhibitor efficacy, with its main components-phenylalanine, tyrosine, DL-ascorbic acid, and apigenin-enabling the adsorption reaction and providing lone-pair electrons for interactions with the steel substrate [14]. Ikueba et al. investigated the corrosion inhibition properties of alkaloid extract from *Garcinia* kola seeds on mild steel in 5M H_2SO_4 at temperatures ranging from 30 to 60 °C. Their study revealed that the inhibition is best explained by physical adsorption, as the efficacy of inhibition increased with decreasing temperature [15]. In a related study, Ikueba and his colleagues found that saponins derived from *Gongronema latifolium* (SEGL) exhibited remarkable inhibition properties on mild steel in acidic environments, achieving an inhibition capacity of 93.7 % at 30 °C with a concentration of 10 g/L of SEGL [16]. Barreto et al. examined the effectiveness of garlic peel extract (*Allium sativum*) in inhibiting corrosion on mild steel using weight loss and electrochemical techniques. Their report showed that a 90.65 % inhibition efficiency was obtained at a 10 v/v% inhibitor concentration [17]. Based on the above references, it can be concluded that the various active groups found in plants have a potent adsorption impact on metal surfaces. Therefore, detailed investigation is needed to understand the complex inhibitory mechanisms, which depend on the different active groups present in the extracts.

Ginger (*Zingiber officinale*), a member of the Zingiberaceae family, is widely cultivated worldwide. It offers significant benefits due to its affordability, non-toxic nature, and widespread availability, making it a popular choice as a food spice or flavoring agent globally. Ginger also has a history of medicinal use, particularly in Southeast Asian countries, for treating ailments such as headaches, colds, rheumatism, fever, and digestive problems [18,19]. Ginger extract contains a variety of bioactive compounds, such as 6-shogaol, 6-gingerol, and zingerone, which are rich in phenolic groups. The π-electrons available in the aromatic ring system further enhance the inhibitory effectiveness of ginger extract [20,21]. Although some studies have explored the efficacy of ginger extracts in inhibiting corrosion on different metals in various environments [22–24], there is insufficient computational data available, which is crucial for theoretically understanding its corrosion inhibition process. Molecular dynamics and quantum mechanical simulations provide this essential information [25–28]. The comprehensive data regarding the effectiveness of ginger in preventing corrosion will provide crucial insights for determining whether it may serve as a viable substitute for the commonly used harmful corrosion inhibitors in the industry.

This study aims to address this gap by employing a comprehensive experimental and theoretical approach to examine the inhibitory effect of ginger extract on mild steel corrosion in a highly acidic solution using the weight loss method. The kinetic and thermodynamic parameters were assessed within the temperature range of 303–333 K. The adsorption phenomena and the presence of different functional groups were verified using UV–Vis and FT-IR spectroscopic techniques. Quantum parameters were generated through molecular dynamic simulations to validate the experimental results.

2. Materials and method

2.1. Materials

Mild steel sheet utilised in this experiment is made up of 98.34 % iron (Fe), 0.08 % carbon (C), 0.26 % silicon (Si), 0.64 % sodium (Na), 0.05 % sulphur (S), 0.09 % nickel (Ni), 0.02 % molybdenum (Mo), 0.08 % chromium (Cr), and 0.27 % copper (Cu). The mild steel was cut into sheets measuring 2.0 cm × 4 cm x 0.08 cm and thereafter polished to obtain a reflective surface using emery paper of several grades, from 600 to 1200. Afterward, the sheets were cleaned of grease utilizing acetone and subsequently placed in a desiccator for storage. The acid test solution (5M H_2SO_4) was prepared using analytical grade H_2SO_4 obtained from Sigma – Aldrich.

2.2. Preparation of inhibitor

Ginger rhizomes were cleaned with distilled water and oven-dried at 50 °C. The dried rhizomes were ground into a fine powder. Ginger root extract (GRE) was extracted from 1 kg of dry powder in 100 % ethanol for 48 h. The extract was concentrated with a vacuum evaporator and dried in a steam bath to produce an ethanol-free solid. The inhibitor test solution of ginger root (GRE) was made by putting 10 g of the GRE in 500 mL of a 5.0 M solution of H_2SO_4. Once prepared, the inhibitor test solution was rapidly agitated and left undisturbed for a duration of 24 h prior to being filtered and finally stored. The stock solution was serially diluted to 0.5, 1.0, 2.5, 5.0, and 10.0 g/L in order to prepare the test solutions for the inhibitor.

2.3. Procedure for weight loss experiment

An analytical balance was used to measured the weight of the mild steel coupons before and after they were suspended in 100 mL of 5M H_2SO_4. The coupon sample was immersion in an H_2SO_4 solution for three consecutive hours at different temperatures (303, 313, 323, and 333 K). This process was carried out both with and exclusive of varying concentrations of ginger extract (0.5, 1.0, 2.5, 5.0, and 10.0 g/L).

Using weight loss data, inhibition efficiency (IE %) as well as the surface coverage (SC) (θ) were calculated using equations (1) and (2) below [11,16]:

$$IE(\%) = \frac{W_o - W_i}{W_o} \times 100 \tag{1}$$

$$\theta = \frac{W_o - W_i}{W_o} \tag{2}$$

Such that w_o and w_i denote weight loss without and with GRE. The rate of corrosion (CR) in the presence and absence of varying GRE concentrations were computed from equation (3) as follows [11]:

$$CR\ (mgcm^{-2}h^{-1}) = \frac{\Delta W}{At} \tag{3}$$

The symbol ΔW represents the amount of weight loss, A represents the surface area of the steel exposed in square centimetres, and t represents the duration of immersion (hrs).

2.4. Sample characterization

The characterization of ginger root extract (GRE) was conducted with Fourier-transform infrared (FT-IR) spectroscopy, Gas chromatography–mass spectrometry (GC-MS) [Thermo GC Trace Ultra Version: 5.0 and Thermo MS DSQ II], and UV–Visible spectroscopy studies. The UV–Visible and FT-IR analysis were performed to identify the electronic transition and functional groups in the GRE solution (10 g/L + 5.0 M H_2SO_4) before and after immersing mild steel for 3 h. This was done to verify the effectiveness of GRE in adsorption and its potency to inhibit corrosion of the steel. The sample solution was analysed using an IS50 FT-IR spectrometer from Thermo Scientific, Waltham, to record the spectra wavelength in the range of 400–4000 cm^{-1}. Additionally, the UV–visible absorption spectra were obtained using a Jenway 7205 UV–Visible Spectrophotometer. The UV–visible absorption spectra were obtained using a Jenway 7205 UV–Visible Spectrophotometer to analyse the spectra of the GRE solution (10 g/L + 5.0 M H_2SO_4) before and after immersing the mild steel for 3 h.

2.5. Computational details

Quantum chemical computations were conducted to establish a relationship between experimental findings and theoretically computed parameters. Density functional theory (DFT) was used to calculate parameters of quantum. The Becke's (B3) parameter exchange functional and Lee Yang Parr's (LYP) gradient corrected correlation dispersion (B3LYP-D3) functional with a 6–311++G(d, p) basis set were used to compute the geometrical optimizations of the studied GRE molecules (neutral and protonated). These

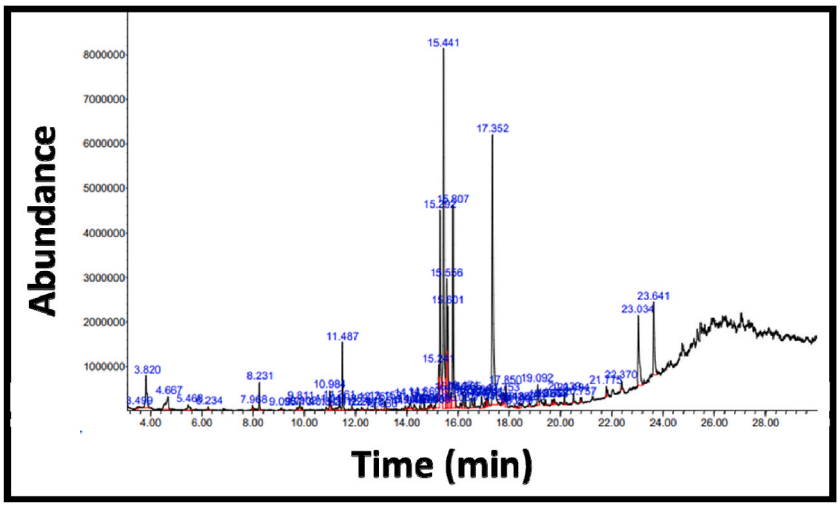

Fig. 1. GC-MS chromatogram of ginger extract.

optimizations were carried out using the Gaussian 16 program package. An investigation of the frontier molecular orbitals (HOMO or LUMO) was conducted, from which significant quantum characteristics were computed, including the global softness (σ), hardness (η, and energy band gap (ΔE). GRE molecules adsorption onto mild steel was simulated with the adsorption locator module of Material Studio program, which utilizes COMPASS for force field approximations.

3. Results and discussion

3.1. Chemical composition of ginger roots extract

3.1.1. GC-MS analysis

The constituents of the ginger extract were identified using GC-MS analysis. The GC-MS chromatogram of the ethanolic extract of ginger root is shown in Fig. 1, with the tentative chemical composition, retention time, base peak, and respective molecular weights summarized in Table 1. The analysis confirms a significant presence of phenolic compounds in the extract. The chromatograms reveal the spectra of four major phenolic constituents (6-Gingerol, 6-Isoshogaol, Zingerone, and Vanylglycol), along with two additional natural compounds (α-Farnesene and β-Bisabolene). Among these, 6-Gingerol, the most active and abundant constituent, was selected for computational studies. The high activity and abundance of 6-Gingerol in ginger have been well-documented in the literatures [18,19,23]. Comparison of the mass spectra with the NIST library showed that the identified compounds displayed well-defined peaks matching their molecular structures, as depicted from the mass spectrograms of GRE in Fig. 2a: 6-Gingerol; b: 6-Isoshogaol; c: Zingerone; d: Vanylglycol; e: ∝- Farnesene; f: β-Bisabolene. The identified compounds align with those previously reported, with 6-Gingerol being a key contributor to the corrosion inhibition properties of ginger root extract (GRE) due to its effective adsorption on the steel surface [18,19,23]. This suggests that the adsorption mechanism of ginger extract involves the oxygen atoms in the C-O bonds of the phenolic groups, which provide lone-pair electrons to form coordinate bonds with the empty d-orbitals of the iron atoms. Consequently, these organic compounds exhibit strong adsorption onto the MS surface [18,19,24].

3.2. Corrosion inhibition evaluation: weight loss experiment

3.2.1. GRE concentration effect

Weight loss approach of measuring metal corrosion is employed due to its ease of use and reliability, particularly in long-term corrosion trials investigations since they do not considerably disrupt the system and enable the tracking of inhibition of corrosion process of the mild steel over time. The reduction in mass of a metal occurs because of the rate of corrosion of the metal, which is caused by the release of hydrogen at the cathode, while the anodic end undergoes oxidation. Fig. 3a-c and 3(d-f) show the correlation between the effectiveness of inhibition and corrosion rate using various concentrations of GRE (in the range of 0–10 mg/L) at varying temperatures (303–333 K) for duration of 1–3 h. The rate of corrosion, inhibitory efficiency, and surface coverage are also displayed in Tables (2–4). When GRE was added to acidic solution, it caused a decrease in the rate at which mild steel corrodes. This is evident from the observation that a rise in GRE concentration results to a decrease in both the corrosion rate and mass loss.

The investigation revealed a strong correlation between the concentration of ginger extract and both the surface coverage and the percentage inhibition efficiency. This indicates that the effectiveness of ginger extract in inhibiting corrosion is influenced by its concentration, as observed in previous studies on general corrosion inhibitors [20–22].

Similar trends were noted while investigating the impact of varying GRE concentration on mild steel corrosion under different temperatures and immersion durations. The maximum inhibitory efficiency was seen at 303 K and an immersion time of 1 h for concentration of GRE between 0.5 mg/L to 10 mg/L. The inhibitory efficiencies for these concentrations were 44.1 %, 58.8 %, 69.0 %, 74.6 %, and 81.3 %, respectively. The rise in inhibitory efficiency with GRE amount is because of the adsorption and greater coverage of the ginger extract on the metal surface, which leads to the formation of a protective barrier layer or film. This film reduces the rate at which the substrate corrodes [20–22].

3.2.2. Effect of temperature

Temperature impact on GRE's potency to contain corrosion on mild steel in 5 M H_2SO_4 was examined for one to 3 h, both with and without GRE, at temperatures between 303 and 333 K. Tables (2–4) revealed how temperature alters corrosion rate of the MS. It is noticed that the CR of metal and the degree of weight loss of the metal increases with raising the temperature because of the anticipated

Table 1
Identified phytochemical constituents of *Zingiber officinalis* using GC-MS.

Comp.	Name	Molecular formula	Molecular Weight $[M]^+$	Base Peak	Retention Time
1	6-Gingerol	$C_{17}H_{26}O_4$	294.38	137	18.799
2	6-Isoshogaol	$C_{17}H_{24}O_3$	276.40	177	23.034
3	Zingerone	$C_{11}H1_4O_3$	194.23	137	17.352
4	Vanylglycol	$C_9H_{12}O_4$	184.19	153	17.684
5	∝- Farnesene	$C_{15}H_{24}$	204.35	41	15.556
6	*β*-Bisabolene	$C_{15}H_{24}$	204.35	69	15.601

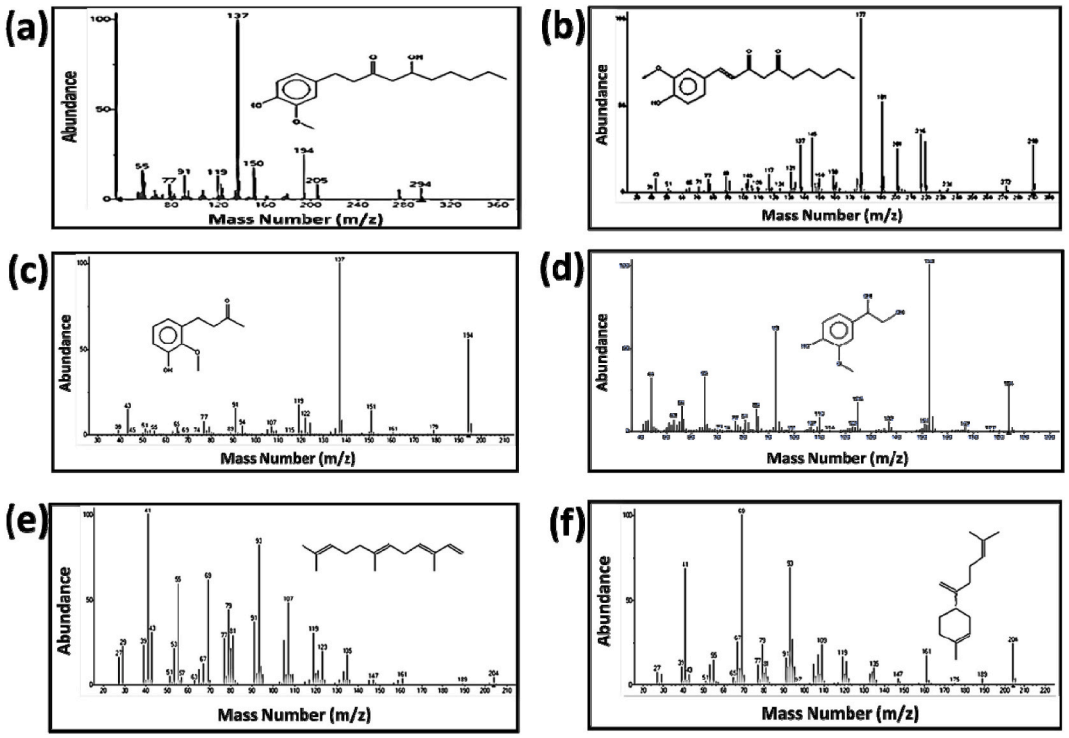

Fig. 2. Mass spectrograms of GRE (a: 6-Gingerol; b: 6-Isoshogaol; c: Zingerone; d: Vanylglycol; e: ∝- Farnesene; f: β-Bisabolene).

rise in chemical dissolution of MS produced by thermal activation [15,17]. The efficiency of inhibition and surface coverage diminish as temperature increases to 333 K, which points to a reduction in GRE's ability to inhibit corrosion of MS at high temperatures. This shows that GRE molecules are physically adsorbed on the surface of MS [23], possibly as a result of the weakly held inhibitor (GRE) desorbing from the metal surface following a significant temperature rise from 303 to 323 K and 1–3 h. One hour of immersion in 10 mg/L GRE exhibits the highest inhibitory efficacy at 303–333 K, with values of 81.3 %, 73.4 %, 65.8 % and 61.3 %, respectively, when compared to other immersion times. To further our comprehension of the complex interactions between GRE and the surface of MS, we subjected the experimental data to additional thermodynamic examinations.

3.3. Thermodynamic investigations

Thermodynamic features, like entropy of activation (ΔS), enthalpy (ΔH), and activation energy (Ea), can offer further understanding of how GRE interacts with the MS surface. The energy of activation was computed from the Arrhenius equation, whereas ΔH and ΔS were derived using the Eyring's equation (equations (4) and (5)).

$$\mathrm{In}Cr = \mathrm{In}A - \frac{E_a}{RT} \tag{4}$$

$$\frac{CR}{T} = \mathrm{In}\frac{K}{Nh} + \frac{\Delta S}{R} + -\frac{\Delta G}{RT} \tag{5}$$

Such that the frequency factor is denoted as A, the activation energy is denoted as E_a, T is the temperature, R is the gas constant, N denotes Avogadro's number; and h represents Plank's constant. The plot of log CR versus 1/T and Eyring's plot (log CR/T versus 1/T) at two (2) hours immersion are shown in Figs. 4 and 5. For the Arrhenius and transition state plots, linear curves with slopes of −ΔEa/2.303R and − ΔH*/2.303R were obtained; these slopes were then used to calculate Ea and H*, which are shown in Table 5. The values of S* indicated in Table 5 were obtained by computing the intercept of [log (R/Nh) + (S*/2.303R)] in Fig. 5. The Ea value without the presence of GRE is 59.65 kJ/mol, whereas the Ea values with GRE varied between 67.89 and 80.26 kJ/mol. With greater Ea values of the inhibitor compared to the Ea value in the absence of the inhibitor, suggest that the mild steel's surface physically adsorbed the GRE molecule [16,23]. The calculated enthalpy change (ΔH) values, both with and without inhibitor, are positive. This confirms the steel corrosion process to endothermic, and the existence of GRE slows down the process of corrosion [23]. Conversely, ΔS value was found to be negative when the GRE inhibitor was present. When ΔS is negative in the presence of GRE, it indicates that the activated complexes in the rate-determining step resolve the issue of dissociation, which results in a decrease in disorderliness as the reactants move into the activated complex. Similar patterns were seen in the Arrhenius and transition state plots (Table S8), which resulted in linear curves after 3 h of immersion.

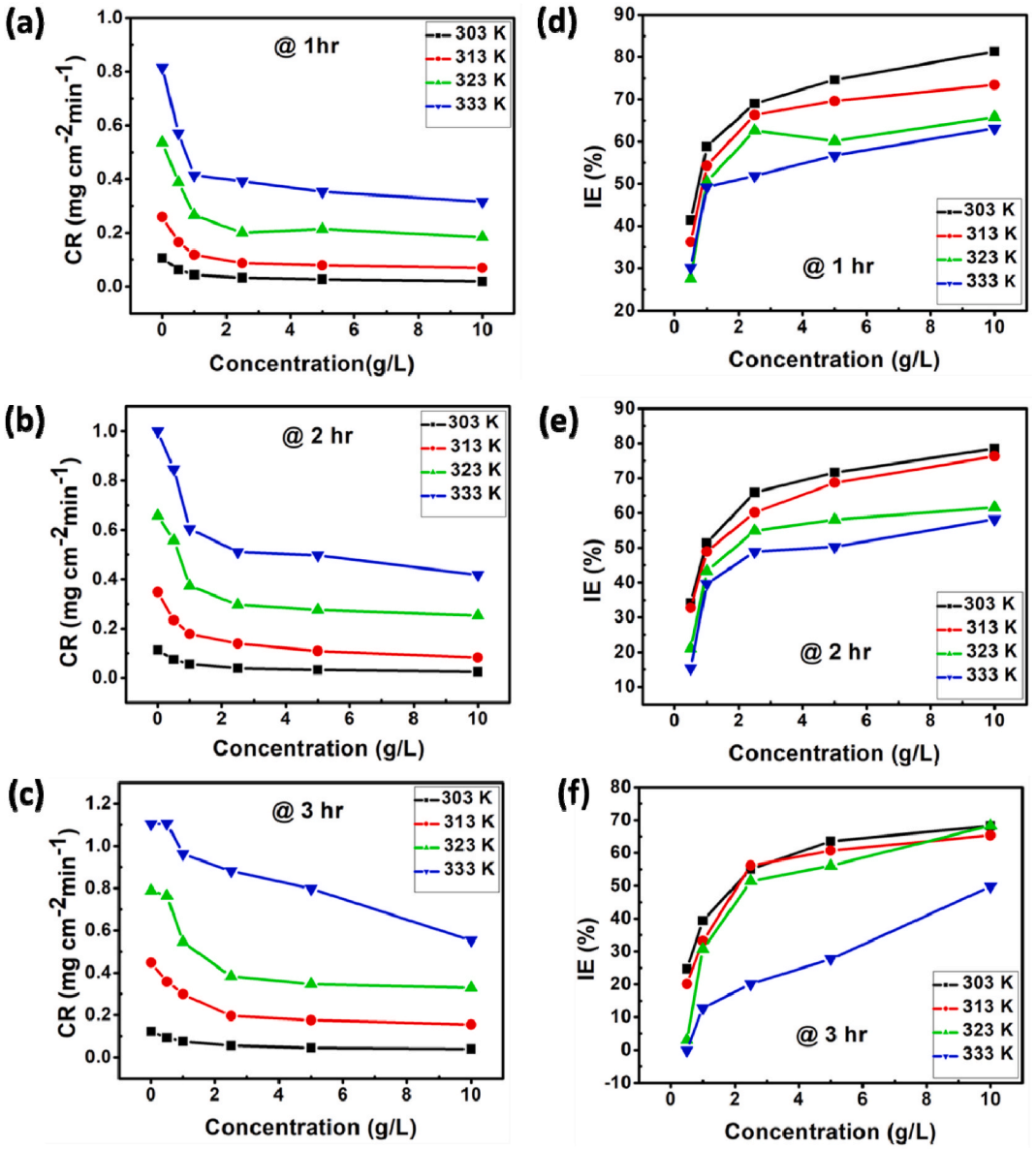

Fig. 3. Variation of (a–c) CR and (d–e) IE (%) of GRE with inhibitor concentration in 5M H_2SO_4 at various temperatures and immersion times.

Table 2
Calculated CR, SC and IE with and without GRE @ 1 h.

Conc.	CR (mg/cm^2/min^1)				SC (θ)				IE (% IE)			
	30 °C	40 °C	50 °C	60 °C	30 °C	40 °C	50 °C	60 °C	30 °C	40 °C	50 °C	60 °C
Blank	0.1060	0.2588	0.5361	0.8155								
0.5	0.0621	0.1651	0.3881	0.5700	0.414	0.362	0.276	0.301	41.4	36.2	27.6	30.1
1.0	0.0437	0.1183	0.2654	0.4143	0.588	0.543	0.505	0.492	58.8	54.3	50.5	49.2
2.5	0.0329	0.0872	0.2005	0.3923	0.690	0.663	0.626	0.519	69.0	66.3	62.6	51.9
5.0	0.0269	0.0787	0.2139	0.3531	0.746	0.696	0.601	0.567	74.6	69.6	60.1	56.7
10.0	0.0198	0.0688	0.1835	0.3156	0.813	0.734	0.658	0.613	81.3	73.4	65.8	61.3

Table 3
Calculated CR, SC and IE with and without GRE @ 2 h.

Conc.	CR (mg/cm^2/min^1)				SC (θ)				IE (% IE)			
	30 °C	40 °C	50 °C	60 °C	30 °C	40 °C	50 °C	60 °C	30 °C	40 °C	50 °C	60 °C
Blank	0.1131	0.3482	0.6578	0.9999								
0.5	0.0744	0.2340	0.5572	0.8469	0.342	0.328	0.211	0.153	34.2	32.8	21.1	15.3
1.0	0.0550	0.1779	0.3730	0.6039	0.514	0.489	0.433	0.396	51.4	48.9	43.3	39.6
2.5	0.0386	0.1386	0.2967	0.5110	0.6.9	0.602	0.549	0.489	65.9	60.2	54.9	48.9
5.0	0.0320	0.1090	0.2756	0.4970	0.717	0.687	0.581	0.503	71.7	68.7	58.1	50.3
10.0	0.0243	0.0825	0.2526	0.4180	0.785	0.763	0.616	0.582	78.5	76.3	61.6	58.2

Table 4
Calculated CR, SC and IE with and without GRE @ 3 h.

Conc.	CR (mg/cm^2/min^1)				SC (θ)				IE (% IE)			
	30 °C	40 °C	50 °C	60 °C	30 °C	40 °C	50 °C	60 °C	30 °C	40 °C	50 °C	60 °C
Blank	0.1226	0.4479	0.7884	1.1037								
0.5	0.0923	0.3579	0.7645	1.1056	0.247	0.201	0.030	−0.017	24.7	20.1	3.03	−0.17
1.0	0.0743	0.2992	0.5464	0.9624	0.394	0.332	0.307	0.128	39.4	33.2	30.7	12.8
2.5	0.0551	0.1962	0.3832	0.8819	0.551	0.562	0.514	0.201	55.1	56.2	51.4	20.1
5.0	0.0446	0.1760	0.3461	0.7980	0.636	0.607	0.561	0.277	63.6	60.7	56.1	27.7
10.0	0.0390	0.1550	0.3461	0.5541	0.682	0.654	0.583	0.498	68.2	65.4	58.3	49.8

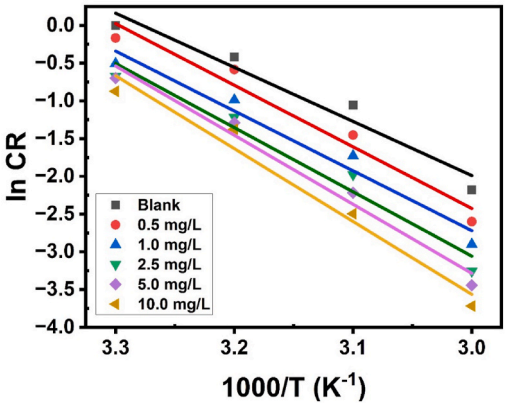

Fig. 4. Arrhenius plot for mild steel corrosion study in 5 M H_2SO_4 solution with and without GRE.

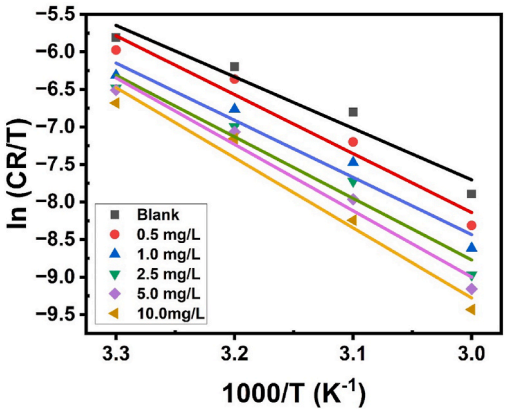

Fig. 5. Transition state plots for mild steel corrosion study in 5 M H_2SO_4 solution with and without GRE.

Table 5
Thermodynamic features for mild steel corrosion study with and without GRE @ 2 h.

Conc. (g/L)	Ea (kJ/mol)	ΔH (kJ/mol)	ΔS (J/mol/K)
Blank	59.65	57.03	22.55
0.5	67.89	65.26	−5.80
1	65.92	63.30	−2.39
2.5	70.76	68.14	−19.69
5	76.12	73.51	−37.64
10	80.26	77.65	−52.41

3.4. Characterization of inhibitor–Fe interaction

3.4.1. IR spectral studies

To better understand how the inhibitor molecule interacts with the metal surface and to characterize the bonding mechanism of inhibitor–Fe interaction complex that forms when the steel coupon is immersed in the GRE inhibitor, FT-IR analysis was employed to identify the specific functional groups present in GRE. The FT-IR spectra of the extract of pure GRE and the GRE extract with corrodents are displayed in Fig. 6. The results observed demonstrate that inhibition of corrosion occurs via an adsorption mechanism. The pure GRE spectrum has large peaks at specific wavenumbers, namely 3355, 2117, 1633, and 1036 cm^{-1}. These peaks represent the stretching vibrations of O–H, C ≡ C, C=C, and C–O in phenol/alcohol, respectively. The immersing mild steel in the extract caused a shift in its spectrum with new peaks observed at 3405, 3024, 2023, 1625, and 1006 cm^{-1} assigned to O–H, C–H, C ≡ C, C=C, and C–O functional groups, which eventually resulted into the formation of a corrosion product, as seen in Fig. 6.

This indicates that there is an inhibitory interaction between the steel substrate and the extract. The spectra show shifts that are as a result of the extracts and mild steel interacting, which is made possible by the functional groups that are in the extracts. It is therefore demonstrable that the functional group and the Fe^{2+} atom present on the surface of metal have bonded to form a coordination bond. This leads to the formation of a Fe^{2+} extract complex on the surface of metal, which ultimately hinders the corrosion of the metal coupon. The obtained FT-IR results are similar with the values reported in the literature [19,23,24].

3.4.2. UV–visible analysis

Fig. 7 displays the UV spectra of the pure GRE extract both before and after immersion in mild steel. A change in the GRE spectrum was observed after immersion, in comparison to the spectrum before to immersion. The GRE's electronic absorption spectra prior to immersion show absorption peaks at 282 nm and 310 nm, respectively. These can be attributed to the π-π* and n-π* transitions, which are caused by the unsaturated nature of the ginger components. Following a 3-h exposure, a noticeable change in the absorbance values was recorded, suggesting the possibility of the inhibitor-Fe complex formation and the subsequent prevention of steel corrosion [19,29,30].

3.5. Computational details

3.5.1. Quantum chemical parameters and optimization

The computational methodology, along with quantum chemistry calculations, was employed to gain deeper insights into the

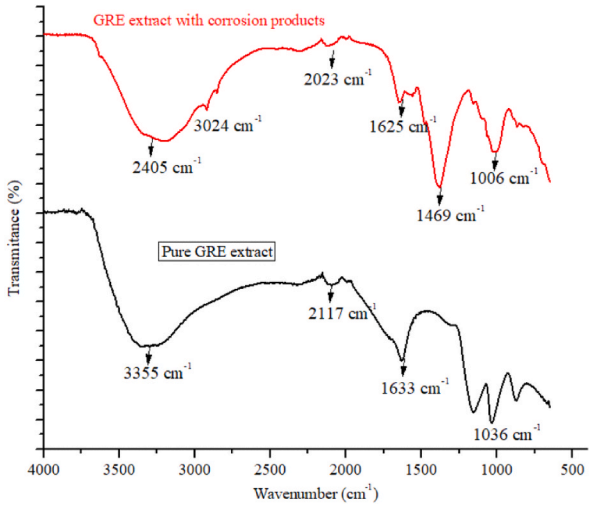

Fig. 6. FT-IR spectra of the extract of pure GRE and the GRE extract with corrodent.

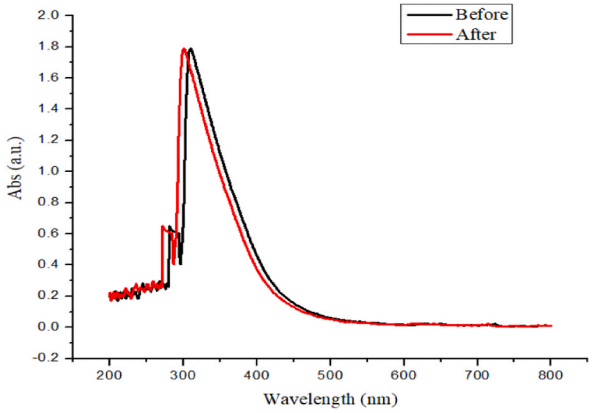

Fig. 7. UV–visible spectra of GRE before and after 3 h of immersion of mild steel.

molecular characteristics of GRE and its potential adsorption mechanism on the mild steel surface. Among the prominent components of GRE, 6-gingerol was selected for quantum chemical analysis. Quantum calculations were performed to determine the frontier molecular orbitals (FMO) of 6-gingerol. Since the FMO is directly related to the energy values of the highest occupied molecular orbital (HOMO) and the lowest unoccupied molecular orbital (LUMO), other descriptors such as ionization energy (IP), electron affinity (EA), electronegativity, chemical hardness (η), energy band gap (ΔE), and softness (σ) were calculated from the FMO using equations (6)–(11) [31–34].

$$\Delta E = E_{LUMO} - E_{HOMO} \tag{6}$$

$$IP = -E_{HOMO} \tag{7}$$

$$EA = -E_{LUMO} \tag{8}$$

$$\chi = \frac{IP + EA}{2} \tag{9}$$

$$\eta = \frac{IP - EA}{2} \tag{10}$$

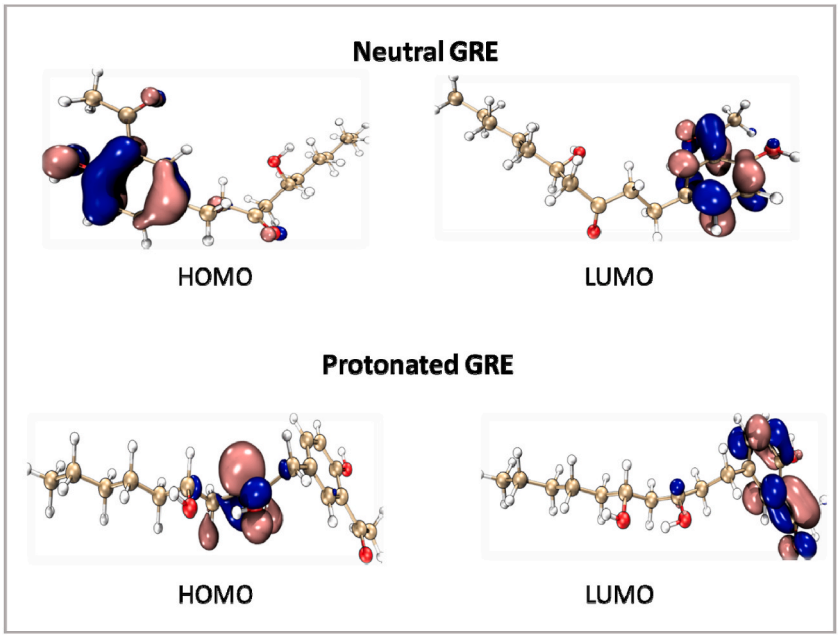

Fig. 8. The HOMO and LUMO orbital visualization of the neutral and the protonated GRE.

$$\sigma = \frac{1}{\eta} \tag{11}$$

Fig. 8depicts the HOMO and LUMO orbital visualization of the neutral and the protonated GRE. According to FMO theory, the HOMO orbital represents the electron-donating propensity of the molecule, while the LUMO orbital corresponds to the molecule's electron-accepting capability [35–40]. The neutral 6-gingerol molecule (n-GRE) exhibits strong localization of electron clouds in both its HOMO and LUMO orbitals on the benzene ring, extending across the carbon-carbon atoms of the aromatic ring. For the 6-gingerol molecule in protonated state (GRE-H$^+$), the electron clouds in both HOMO and LUMO orbitals are primarily concentrated on the benzene ring and the hydroxyl group. This suggests that the enhanced inhibitory effect of GRE-H$^+$ can be attributed to the presence of aromatic groups containing π-electrons, oxygen heteroatoms, and the hydroxyl group, which are productive adsorption sites capable of forming chemical coordination interactions with metal surfaces [35–40].

To also evaluate the inhibitory effectiveness of 6-gingerol, the energy band gap (ΔE) is calculated as the energy difference between the HOMO and LUMO orbitals of the 6-gingerol. As shown in Table 6, the protonated 6-gingerol molecule (GRE-H$^+$) demonstrates higher suppression of mild steel (MS) corrosion compared to 6-gingerol in the neutral state (n-GRE), which is associated with a lower ΔE value. A smaller ΔE value indicates a greater likelihood of 6-gingerol undergoing protonation before adsorbing onto metal surfaces [41–43]. Furthermore, ionization potential (IP) and electron affinity (EA) are critical parameters for assessing the corrosion inhibition performance of GRE. Optimal anti-corrosion performance is characterized by lower IP and higher EA values [44–46]. GRE-H$^+$, with an IP of 6.286 eV and an EA of 0.366 eV, exhibits superior corrosion resistance compared to n-GRE, which has an IP of 8.338 eV and an EA of 0.247 eV.

Additional computed parameters, such as chemical hardness (η) and softness (σ), also play significant roles in determining the reactivity and inhibition effectiveness of GRE. Chemical hardness assesses the structural stability of the active component, 6-gingerol, within the GRE composite. The low chemical hardness (η) of GRE-H$^+$ indicates its efficacy as a corrosion inhibitor. Conversely, chemical softness (σ), which is the reciprocal of hardness (η), exerts an opposite effect on corrosion inhibition [44–46]. Although GRE-H$^+$'s low chemical hardness value confirms its superior inhibitory capacity compared to neutral 6-gingerol (n-GRE), its high chemical softness value further enhances its protective effectiveness as a corrosion inhibitor.

Moreover, the dipole moment (μ), which defines the molecular polarity of the inhibitors [47,48], is higher in GRE-H$^+$ than in n-GRE. This suggests that the protonated 6-gingerol molecule (GRE-H$^+$) has a greater propensity to donate electrons to the metal surface, thereby demonstrating its superior capability in inhibiting corrosion [47,48].

3.5.2. Molecular electrostatic potential

To better understand and illustrate the distribution of electron density in the HOMO and LUMO orbitals of both protonated and neutral species of GRE, molecular electrostatic potential (MEP) analysis was employed. MEP is often used to predict the reactive sites of a molecule, particularly in electrophilic and nucleophilic reactions [49,50]. The traditional colour scale for MEP surfaces is as follows: blue indicates electron-poor areas (positive charge), while red represents electron-rich areas (negative charge) [25,51,52]. As shown in Fig. 9, the blue regions are distributed along the carbon bond moiety in both GRE and GRE-H$^+$ species, while the red regions are concentrated around negatively charged groups containing heteroatoms, such as oxygen atoms, and around certain carbon atoms in the inhibitor molecule. The MEP maps reveal the reactive sites of the inhibitors; for protonated GRE-H$^+$, oxygen atoms are shown to be the primary adsorption sites. Therefore, it can be inferred that the corrosion inhibitor under investigation becomes more active upon protonation [25,44,49–52].

3.5.3. Molecular dynamics simulation (MD)

The MD simulation was conducted to achieve the equilibrium adsorption of GRE on the Fe (110) surface at temperatures of 303 K and 333 K, while using the experimental conditions Fig. 10 shows both the top and side views of the inhibitor molecule's ideal adorable adsorption configuration in an acidic and neutral state when the GRE molecules adsorbed at 303 K and 333 K.

The image illustrates how both protonated (acidic state) and non-protonated (neutral state) configurations of GRE cover the whole iron surface Fe (110), suggesting that the compound under investigation has more active sites. The binding energies derived from the molecular dynamic simulation are shown in Table 7.

The results demonstrate that the inhibitor molecules maintained a flat-lying adsorption orientation on the Fe (110) surface, as evidenced by the delocalization of electron density across both protonated and neutral GRE molecules at 303 K and 333 K. This configuration enhances surface contact between the molecule and the metal surface, thereby contributing to corrosion inhibition. It has been reported that more negative binding energy ($E_{binding}$) values indicate stronger interactions between the inhibitor and the iron surface, which correlates with higher inhibition efficacy [51–53]. At 303 K, both neutral and protonated GRE exhibited negative $E_{binding}$ values, indicating better adsorption of the inhibitor onto the metal surface and, consequently, higher inhibition. In contrast, the positive $E_{binding}$ values at 333 K for both neutral and protonated GRE suggest the possible desorption of the adsorbed inhibitor from the metal surface at elevated temperatures. The calculated interaction energies at various temperatures are displayed in Table 7, with the highest value of −4.736 kJ/mol occurring at 303 K. This suggests that the acidified GRE compound exhibits a stronger ability to provide protection against corrosion compared to other states. Fig. 11 illustrates the corrosion mechanism by showing how GRE molecules attach to the mild steel substrate through the oxygen atom in the C=O, O-H group, and aromatic OH part of the GRE heteroatoms.

Table 6
Calculated HOMO, LUMO, Energy gap, chemical hardness and softness and chemical potential values computated at the B3LYP-GD3BJ/def2tzvp level of theory.

Inhibitor	E_{HOMO} (eV)	E_{LUMO} (eV)	ΔE_{gap} (eV)	IP(eV)	EA(eV)	χ (eV)	η (eV)	σ (eV^{-1})	μ(eV)
Protonated GRE	−6.286	−0.366	5.920	6.286	0.366	3.326	5.920	0.169	2.96
Neutral GRE	−8.338	−0.247	8.091	8.338	0.247	4.293	4.045	0.233	4.046

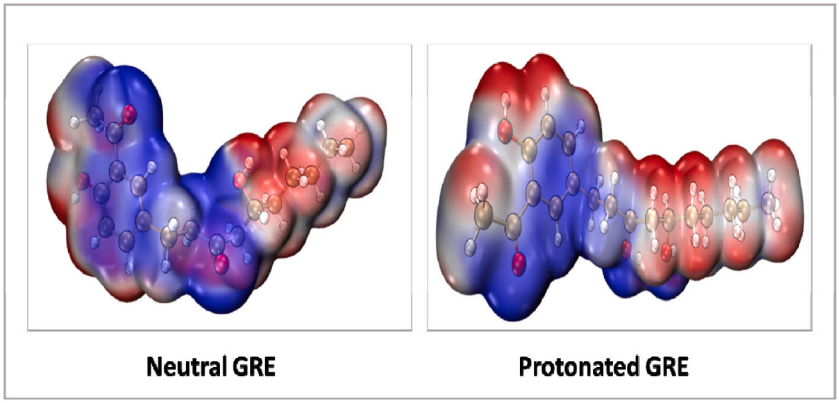

Fig. 9. Molecular electrostatic potential of the GRE, in neutral and protonated states.

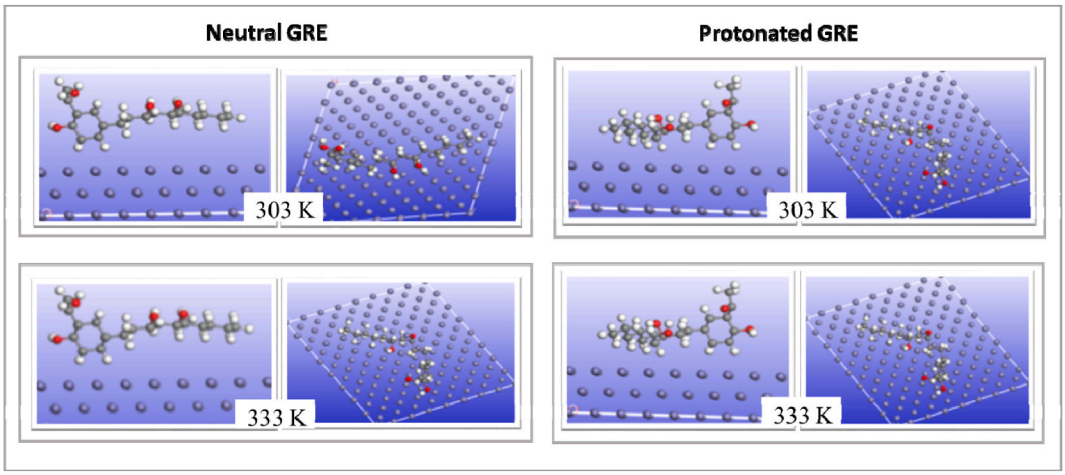

Fig. 10. The equilibrium adsorption configuration of Side and top view for the neutral and protonated inhibitor species on the Fe (110) surface at temperature of 303 K and 333 K.

Table 7
Binding energies of protonated and neutral ginger species on mild steel at temperature of 3003 K and 333 K.

Temperature (K)	$E_{binding}$ (KJ/mol)	
	Neutral GRE	Protonated GRE^{+}
303	−4.555	−4.736
333	0.05	0.06

4. Conclusion

The study investigates the effectiveness of ginger root extract (GRE) as a corrosion inhibitor for mild steel in a 5 M H_2SO_4 solution across temperatures ranging from 303 to 333 K, using both theoretical and experimental approaches. The results from weight loss

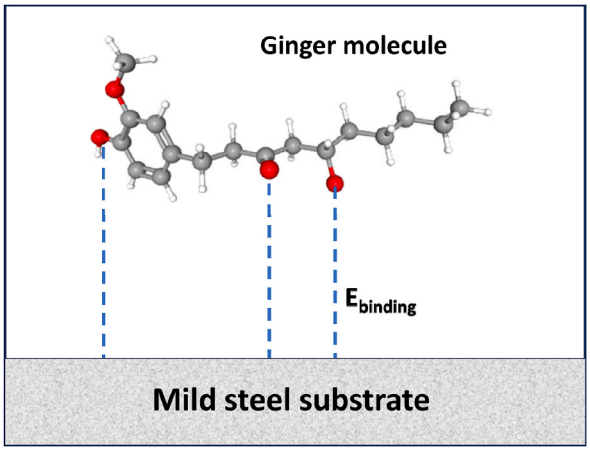

Fig. 11. Schematic depiction of corrosion mechanism portraying the mode of adsorption of molecules of ginger onto the MS substrate.

experiments showed that GRE significantly reduces the corrosion of mild steel in acidic environments, with inhibition efficiency (IE%) increasing as GRE concentration increases, temperature decreases, and immersion time is minimized. The highest inhibitory efficiency, 81.3 %, was observed at a concentration of 10 mg/L at 303 K for 1 h. The thermodynamic activation parameters suggested that the corrosion inhibition process is temperature-dependent, and alignment with the Langmuir isotherm indicated that GRE molecules adhere to the surface of MS through a physical adsorption mechanism. Also, GC-MS results revealed four major phenolic compounds—6-gingerol, 6-isoshogaol, zingerone, and vanillyl glycol—and two secondary metabolites, α-Farnesene and β-Bisabolene. Among these, 6-gingerol, the most active and abundant constituent, was chosen for computational studies. Quantum chemistry calculations highlighted the key quantum chemical descriptors, identifying protonated 6-gingerol as the primary molecule responsible for the corrosion inhibition efficiency in GRE, with highly significant interactions between 6-gingerol molecules and surface of the MS. Molecular simulations further revealed that the stable adsorption conformations are predominantly facilitated by the oxygen heteroatoms in 6-gingerol molecules.

Funding

This research was funded by Taif University, Saudi Arabia, project No.(TU-DSPP-2024-13).

Data and code availability

Data will be made available on request.

CRediT authorship contribution statement

Olajire Samson Olanrele: Supervision, Methodology, Formal analysis, Data curation. **Joseph Femi-Dagunro:** Writing – original draft, Methodology, Investigation. **Edwin Andrew Ofudje:** Writing – original draft, Supervision, Data curation, Conceptualization. **Meri Algarni:** Software, Resources, Project administration. **Azza A. Al-Ghamdi:** Software, Resources, Formal analysis. **Reema H. Aldahiri:** Writing – review & editing, Validation, Software. **Mazen R. Alrahili:** Software, Resources, Formal analysis. **Ahad Amer Alsaiari:** Resources, Funding acquisition.

Declaration of competing interest

The authors declare that they have no known competing financial interests or personal relationships that could have appeared to influence the work reported in this paper.

Acknowledgements

The authors extend their appreciation to Taif University, Saudi Arabia, for supporting this work through project number (TU-DSPP-2024-13).

Appendix A. Supplementary data

Supplementary data to this article can be found online at https://doi.org/10.1016/j.heliyon.2024.e37493.

References

[1] S.Z. Salleh, A.H. Yusoff, S.K. Zakaria, M.A.A. Taib, A.A. Seman, M.N. Masri, M. Mohamad, S. Mamat, S.A. Sobri, A. Ali, Plant extracts as green corrosion inhibitor for ferrous metal alloys: a review, J. Clean. Prod. 304 (2021) 127030.
[2] I.-I.N. Etim, D.I. Njoku, P.C. Uzoma, S.K. Kolawole, O.S. Olanrele, O.O. Ekarenem, B.O. Okonkwo, A.I. Ikeuba, I.I. Udoh, C.N. Njoku, Microbiologically influenced corrosion: a concern for oil and gas sector in Africa, Chemistry Africa 6 (2) (2023) 779–804.
[3] A. Obike, K. Uwakwe, E. Abraham, A. Ikeuba, W. Emori, Review of the losses and devastation caused by corrosion in the Nigeria oil industry for over 30 years, International Journal of Corrosion Scale Inhibition 9 (1) (2020) 74–91.
[4] Y. El Kacimi, S. Kaya, R. Touir, New Challenges and Industrial Applications for Corrosion Prevention and Control, IGI Global, 2020.
[5] S.H. Alrefaee, K.Y. Rhee, C. Verma, M. Quraishi, E.E. Ebenso, Challenges and advantages of using plant extract as inhibitors in modern corrosion inhibition systems: recent advancements, J. Mol. Liq. 321 (2021) 114666.
[6] S. Ghaffari, M. Aliofkhazraei, G. Barati Darband, A. Zakeri, E. Ahmadi, Review of superoleophobic surfaces: evaluation, fabrication methods, and industrial applications, Surface. Interfac. 17 (2019) 100340.
[7] C. Verma, E.E. Ebenso, M. Quraishi, C.M. Hussain, Recent developments in sustainable corrosion inhibitors: design, performance and industrial scale applications, Materials Advances 2 (12) (2021) 3806–3850.
[8] S. Umoren, O. Ogbobe, I. Igwe, E. Ebenso, Inhibition of mild steel corrosion in acidic medium using synthetic and naturally occurring polymers and synergistic halide additives, Corrosion Sci. 50 (7) (2008) 1998–2006.
[9] K. Tamalmani, H. Husin, Review on corrosion inhibitors for oil and gas corrosion issues, Appl. Sci. 10 (10) (2020) 3389.
[10] M. Izadi, T. Shahrabi, I. Mohammadi, B. Ramezanzadeh, Synthesis of impregnated Na+-montmorillonite as an eco-friendly inhibitive carrier and its subsequent protective effect on silane coated mild steel, Prog. Org. Coating 135 (2019) 135–147.
[11] T.O. Martins, E.A. Ofudje, A.A. Ogundiran, O.A. Ikeoluwa, O.A. Oluwatobi, E.F. Sodiya, O. Ojo, Cathodic corrosion inhibition of steel by Musa paradisiaca leave extract, Journal of the Nigerian Society of Physical Sciences (2022) 740, 740.
[12] B. Tan, Y. Liu, Z. Gong, X. Zhang, J. Chen, L. Guo, J. Xiong, J. Liu, R. Marzouki, W. Li, Pyracantha fortuneana alcohol extracts as biodegradable corrosion inhibitors for copper in H_2SO_4 media.", J. Mol. Liq. 397 (2024) 124117.
[13] B. Tan, Z. Gong, W. He, J. Xiong, L. Guo, R. Marzouki, Insight into the anti-corrosion mechanism of crop waste Arachis hypogaea L. leaf extract for copper in sulfuric acid medium, Sustainable Chemistry and Pharmacy 38 (2024) 101449.
[14] H. Ren, Y. Liu, Z. Gong, B. Tan, H. Deng, J. Xiong, P. Shao, Q. Dai, J. Cao, R. Marzouki, Pumpkin leaf extract crop waste as a new degradable and environmentally friendly corrosion inhibitor.", Langmuir 40 (11) (2024) 5738–5752.
[15] A. Ikeuba, P. Okafor, U. Ekpe, E.E. Ebenso, Alkaloid and non-alkaloid ethanolic extracts from seeds of Garcinia kola as green corrosion inhibitors of mild steel in H2SO4 solution, Int. J. Electrochem. Sci. 8 (5) (2013) 7455–7467.
[16] A.I. Ikeuba, P.C. Okafor, Green corrosion protection for mild steel in acidic media: saponins and crude extracts of Gongronema latifolium, Pigment Resin Technol. 48 (1) (2019) 57–64.
[17] L.S. Barreto, M.S. Tokumoto, I.C. Guedes, H.G.d. Melo, F.D.R. Amado, V.R. Capelossi, Evaluation of the anticorrosion performance of peel garlic extract as corrosion inhibitor for ASTM 1020 carbon steel in acidic solution, Materia 22 (2017) e11852.
[18] H.K. Shareef, H.J. Muhammed, H.M. Hussein, I.H. Hameed, Antibacterial effect of ginger (Zingiber officinale) roscoe and bioactive chemical analysis using gas chromatography mass spectrum, Orient. J. Chem. 32 (2) (2016) 20–40.
[19] D. Gaikwad, S.K. Shinde, A.V. Kawade, S. Jadhav, M. Gadhave, Isolation and standardization of gingerol from ginger rhizome by using TLC, HPLC, and identification tests, Pharma Innov. 6 (2, Part C) (2017) 179.
[20] M. El-Sabbah, H. Khalil, M. Mahross, B. Mahran, A. Gomaa, Aqueous extract of ginger as green corrosion inhibitor for mild steel in hydrochloric acid solution, Molecules 1 (2015) 2.
[21] B.A. Kurniawan, A. Pradana, S. Sulistijono, S. Sutarsis, Study on ginger extract performance as corrosion inhibitor in acid and neutral environments, Adv. Mater. Res. 896 (2014) 331–334.
[22] A. Fidrusli, M. Mahmood Suryanto, Ginger extract as green corrosion inhibitor of mild steel in hydrochloric acid solution. IOP Conference Series: Materials Science and Engineering, IOP Publishing, 2018 012087.
[23] H. Gadow, M. Motawea, Investigation of the corrosion inhibition of carbon steel in hydrochloric acid solution by using ginger roots extract, RSC Adv. 7 (40) (2017) 24576–24588.
[24] Y. Liu, Z. Song, W. Wang, L. Jiang, Y. Zhang, M. Guo, F. Song, N. Xu, Effect of ginger extract as green inhibitor on chloride-induced corrosion of carbon steel in simulated concrete pore solutions, J. Clean. Prod. 214 (2019) 298–307.
[25] R. Hsissou, S. Abbout, R. Seghiri, M. Rehioui, A. Berisha, H. Erramli, M. Assouag, A. Elharfi, Evaluation of corrosion inhibition performance of phosphorus polymer for carbon steel in [1 M] HCl: computational studies (DFT, MC and MD simulations), J. Mater. Res. Technol. 9 (3) (2020) 2691–2703.
[26] M. Damej, R. Hsissou, A. Berisha, K. Azgaou, M. Sadiku, M. Benmessaoud, N. Labjar, New epoxy resin as a corrosion inhibitor for the protection of carbon steel C38 in 1M HCl. experimental and theoretical studies (DFT, MC, and MD), J. Mol. Struct. 1254 (2022) 132425.
[27] S.O. Olanrele, Z. Lian, C. Si, S. Chen, B. Li, Tuning of interactions between cathode and lithium polysulfide in Li-S battery by rational halogenation, J. Energy Chem. 49 (2020) 147–152.
[28] S.O. Olanrele, Z. Lian, C. Si, B. Li, Halogenation of graphene triggered by heteroatom doping, RSC Adv. 9 (64) (2019) 37507–37511.
[29] J. Jeyasundari, S. Rajendran, R.S. Kannan, Y.B.A. Jacob, Electrochemical and surface analysis studies on corrosion inhibition of carbon steel, Eur Chem Bull 2 (9) (2013) 585.
[30] M. Liu, X. Xia, G. Chou, D. Liu, A. Zuberi, J. Ye, Z. Liu, Variations in the contents of gingerols and chromatographic fingerprints of ginger root extracts prepared by different preparation methods, J. AOAC Int. 97 (1) (2014) 50–57.
[31] M. Orio, D.A. Pantazis, F. Neese, Density functional theory, Photosynth. Res. 102 (2009) 443–453.
[32] N.D. Hine, M. Robinson, P.D. Haynes, C.-K. Skylaris, M.C. Payne, A.A. Mostofi, Accurate ionic forces and geometry optimization in linear-scaling density-functional theory with local orbitals, Phys. Rev. B 83 (19) (2011) 195102.
[33] S.G. Balasubramani, G.P. Chen, S. Coriani, M. Diedenhofen, M.S. Frank, Y.J. Franzke, F. Furche, R. Grotjahn, M.E. Harding, C. Hättig, TURBOMOLE: modular program suite for ab initio quantum-chemical and condensed-matter simulations, J. Chem. Phys. 152 (18) (2020).
[34] T. Mackoy, B. Kale, M.E. Papka, R.A. Wheeler, viewSq, a Visual Molecular Dynamics (VMD) module for calculating, analyzing, and visualizing X-ray and neutron structure factors from atomistic simulations, Comput. Phys. Commun. 264 (2021) 107881.
[35] J. Zhang, F. Zhan, N. Ai-Zaqri, Corrosion inhibition performance of Punica granatum L extract on Q235 steel in H2SO4 environment: electrochemical, morphological, and quantum chemical studies, Int. J. Electrochem. Sci. 18 (10) (2023) 100267.
[36] Y. Cao, H. Shao, S. He, Z. Chen, W. Yang, Natural polycitric acid-curcumin for highly efficient corrosion inhibition of aluminum alloys, Mater. Today Commun. 36 (2023) 106659.
[37] N.M. El Basiony, A. Elgendy, A.E. El-Tabey, A.M. Al-Sabagh, G.M. Abd El-Hafez, M.A. El-raouf, M.A. Migahed, Synthesis,characterization, experimental and theoretical calculations (DFT and MC) of ethoxylated aminothiazole as inhibitor for X65 steel corrosion in highly aggressive acidic media, J. Mol. Liq. 297 (2020) 111940.
[38] B. Nikitiuk, D. Salikova, N. Kondratyuk, V. Pisarev, Pair entropy and universal viscosity scaling for molecular systems via molecular dynamics simulations, J. Mol. Liq. 368 (2022) 120714.
[39] U.G. Chuwkwu, H. Louis, H.O. Edet, T.O. Unimuke, P.O. Olagoke, A.S. Adeyinka, Toward site-specific interactions of n H2 (n= 1–4) with Ga12As12 nanostructured for hydrogen storage applications, Energy Fuels 37 (2) (2023) 1353–1369.
[40] H. Louis, G.E. Mathias, O.J. Ikenyirimba, T.O. Unimuke, D. Etiese, A.S. Adeyinka, Metal-doped Al12N12X (X= Na, Mg, K) nanoclusters as nanosensors for carboplatin: insight from first-principles computation, J. Phys. Chem. B 126 (27) (2022) 5066–5080.

[41] B. El-Haitout, C. Hejjaj, H. Lgaz, M.R. Al-Hadeethi, O.M. Ali, H.S. Lee, I.H. Ali, R. Salghi, Superior long-term corrosion inhibition of N80 steel by new eco-friendly hydrazone-based compounds in a simulated oil well acidizing environment: establishing the mechanism at the molecular level, Langmuir 38 (2022) 15937.
[42] Z. Liu, Q. Chu, H. Chen, Y.J. Qiang, X. Zhang, Y.W. Ye, Experimental and molecular simulation studies of N, S-doped Carbon dots as an eco-friendly corrosion inhibitor for protecting Cu in HCl environment, Colloids Surf., A 669 (2023) 131504.
[43] B. Tan, S. Zhang, W. Li, X. Zuo, Y. Qiang, L. Xu, J. Hao, S. Chen, Experimental and theoretical studies on inhibition performance of Cu corrosion in 0.5 M H2SO4 by three disulphide derivatives, J. Ind. Eng. Chem. 77 (2019) 449–460.
[44] H. Zeng, X. Zhao, Y. Wang, X. Dong, A. Liu, X. Ren, Investigation of the inhibition mechanism of organic corrosion inhibitors on the copper surface by DFT study and MD simulations, ChemistrySelect 8 (23) (2023) e202204908.
[45] A. Abdullahia, A. Muhamma, DFT and molecular dynamic simulation study on the corrosion inhibition of Aluminum by some flavonoids of Guiera Senegalensis leaves, Algerian Journal of Engineering and Technology 4 (2021) 66–73.
[46] R. Oukhrib, Y. Abdellaoui, A. Berisha, H.A. Oualid, J. Halili, K. Jusufi, M. Ait El Had, H. Bourzi, S. El Issami, F.A. Asmary, V.S. Parmar, C. Len, DFT, Monte Carlo and molecular dynamics simulations for the prediction of corrosion inhibition efficiency of novel pyrazolylnucleosides on Cu (111) surface in acidic media, Sci. Rep. 11 (1) (2021) 3771.
[47] C. Ouyang, Z. Wang, B. Tan, A. Brahmia, Insights into the anticorrosion performance of solanum lyratum leaf extract for copper in sulfuric acid medium, Langmuir 39 (19) (2023) 6666–6680.
[48] I. Merimi, R. Aslam, B. Hammouti, T. Szumiata, H. Lgaz, I.-M. Chung, Adsorption and inhibition mechanism of (Z)-4-((4-methoxybenzylidene)amino)-5-methyl-2,4-dihydro-3H-1,2,4-triazole-3-thione on carbon steel corrosion in HCl: experimental andtheoretical insights, J. Mol. Struct. 1231 (2021) 129901.
[49] F. Dismer, M. Petzold, J. Hubbuch, Effects of ionic strength and mobile phase pH on the binding orientation of lysozyme on different ion-exchange adsorbents, J. Chromatogr. A 1194 (1) (2008) 11–21.
[50] W.D. Arnold, E. Oldfield, The chemical nature of hydrogen bonding in proteins via NMR: J-couplings, chemical shifts, and AIM theory, J. Am. Chem. Soc. 122 (51) (2000) 12835–12841.
[51] O.E. Oyeneyin, N.D. Ojo, N. Ipinloju, E.B. Agbaffa, A.V. Emmanuel, Investigation of the corrosion inhibition potentials of some 2-(4-(substituted) arylidene)-1H-indene-1, 3-dione derivatives: density functional theory and molecular dynamics simulation, Beni-Suef University Journal of Basic Applied Sciences 11 (1) (2022) 132.
[52] H. Lgaz, R. Salghi, S. Masroor, S.-H. Kim, C. Kwon, S.Y. Kim, Y.-J. Yang, I.-M. Chung, Assessing corrosion inhibition characteristics of hydrazone derivatives on mild steel in HCl: insights from electronic-scale DFT and atomic-scale molecular dynamics, J. Mol. Liq. 308 (2020) 112998.
[53] A.I. Ikeuba, O.B. John, V.M. Bassey, H. Louis, A.U. Agobi, J.E. Ntibi, F.C. Asogwa, Experimental and theoretical evaluation of aspirin as a green corrosion inhibitor for mild steel in acidic medium, Results in Chemistry 4 (2022) 100543.